SANDIA REPORT
SAND2009-6209
Unlimited Release
Printed September 2009

Neural Assembly Models Derived through Nano-Scale Measurements

Hongyou Fan, Catherine Branda, Christy Warrender, Richard Schiek, Chris Forsythe

Prepared by
Sandia National Laboratories
Albuquerque, New Mexico 87185 and Livermore, California 94550

Sandia is a multiprogram laboratory operated by Sandia Corporation,
a Lockheed Martin Company, for the United States Department of Energy's
National Nuclear Security Administration under Contract DE-AC04-94AL85000.

Issued by Sandia National Laboratories, operated for the United States Department of Energy by Sandia Corporation.

Available to DOE and DOE contractors from
U.S. Department of Energy
Office of Scientific and Technical Information
P.O. Box 62
Oak Ridge, TN 37831

Telephone: (865) 576-8401
Facsimile: (865) 576-5728
E-Mail: reports@adonis.osti.gov
Online ordering: http://www.osti.gov/bridge

Available to the public from
U.S. Department of Commerce
National Technical Information Service
5285 Port Royal Rd.
Springfield, VA 22161

Telephone: (800) 553-6847
Facsimile: (703) 605-6900
E-Mail: orders@ntis.fedworld.gov
Online order: http://www.ntis.gov/help/ordermethods.asp?loc=7-4-0#online

SAND2009-6209
Unlimited Release
Printed September 2009

Neural Assembly Models Derived through Nano-Scale Measurements

Hongyou Fan[1], Catherine Branda[2], Christy Warrender[3], Richard Schiek[4], Chris Forsythe[5]
[1]1815 Ceramic Processing and Inorganic Materials,
[2]8621 Biosystems Research & Development,
[3]6343 Cognitive System Research & Applications,
[4]1437 Electrical and Microsystems Modeling ,
[5]6341 Cognitive & Exploratory Systems

Sandia National Laboratories
P.O. Box 5800
Albuquerque, New Mexico 87185-MS1349

Abstract

This report summarizes accomplishments of a three-year project focused on developing technical capabilities for measuring and modeling neuronal processes at the nanoscale. It was successfully demonstrated that nanoprobes could be engineered that were biocompatible, and could be biofunctionalized, that responded within the range of voltages typically associated with a neuronal action potential. Furthermore, the Xyce parallel circuit simulator was employed and models incorporated for simulating the ion channel and cable properties of neuronal membranes. The ultimate objective of the project had been to employ nanoprobes *in vivo*, with the nematode *C elegans*, and derive a simulation based on the resulting data. Techniques were developed allowing the nanoprobes to be injected into the nematode and the neuronal response recorded. To the authors's knowledge, this is the first occasion in which nanoparticles have been successfully employed as probes for recording neuronal response in an *in* vivo animal experimental protocol.

CONTENTS

FIGURES

1. INTRODUCTION

Neuroscience experimental techniques allow brain activity to be measured at the cellular level (e.g. microelectrode implants) and the large-scale systems level (e.g. EEG, fMRI), however existing methods offer limited insight bridging these scales. For instance, there is little understanding of the mechanisms by which individual neurons are organized into assemblies that correspond to specific memories. Significant scientific advances would be attainable given technology that enables measurement of the activity of individual neurons for large volumes of brain tissue in vivo (i.e. living animal).

The objectives for the Neural Assembly Models Derived through Nano-Scale Measurements LDRD has been to leverage Sandia National Laboratories technical strengths in nanotechnology and high-performance computing to develop innovative capabilities for measuring and modeling neuronal activity. The project was constructed with two parallel paths that converged in the final year of the project to demonstrate an integrative capability for neuronal sensing and modeling. The first path focused on nanoscale neural measurement and built upon earlier groundbreaking successes in applying nanomaterials to sense neural phenomena. The second path addressed computational modeling, adapting the Xyce circuit simulator for modeling and simulation of neural circuits. These paths converged during the final year of the 3-year project using C elegans as an experimental platform.

Over the course of the 3-year project, there were numerous accomplishments culminating in the successful demonstration of the use of nanoprobes to detect neural processes in vivo with C elegans and modeling those same processes within a Xyce simulation. The following sections summarize specific technical developments and accomplishments of the project.

2. NANOPARTICLES

In this project, we have synthesized well-defined monodisperse fluorescent nanoparticles. monodisperseMonodisperse CdSe, PbSe, PbTe nanocrystals of 4-8 nm have been successfully synthesized through a "hot soap" injection process. Shapes have been controlled to be spherical and cubic. We have investigated the influence of crystal structure on the emissions. We optimized optical emission through optimization of crystalline structure. Initial experimental work showed as-prepared nanocrystals had good crystal structures. Annealing treatment at 150˚C resulted in the best crystal structure with near and well-defined X-ray diffraction patterns. Initial optical characterization using absorbance spectroscopy recorded on as-prepared nanocrystal solutions showed the nanocrystals had sharp absorption between 1000-2500 nm, which is ideal for fluorecent or IR imaging. We have biofunctionalized these nanocrystals. Functionalization was accomplished through our recent developeda micellization method. Phospholipids were used to encapsulated the monoidpserse IR nanocrystals within a micelle core to form water-soluble and biocompatible nanocrystal micelles. We also designed and synthesized special ligands to functionalize the nanocrysal surface so that the final nanocrystals allow further conjugation with small peptides etc. (see Fig 1)

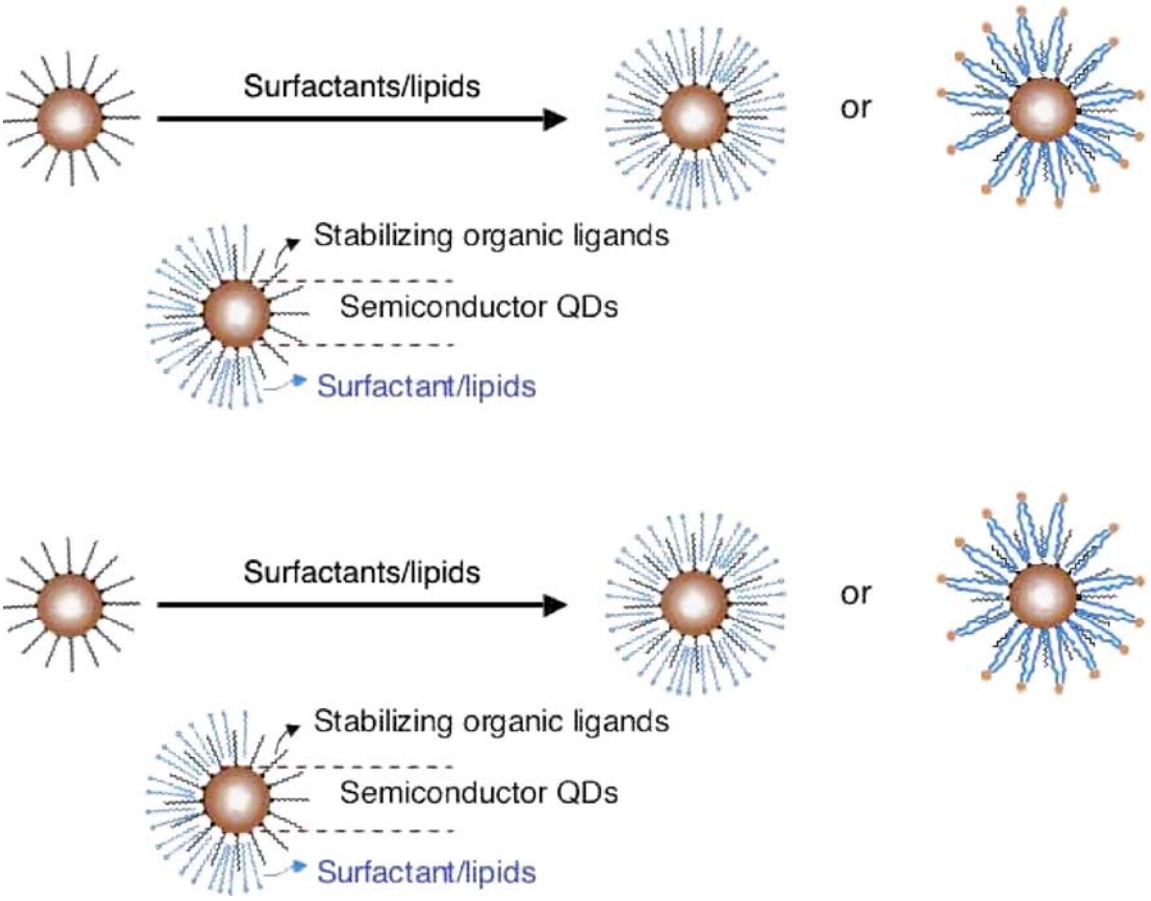

Figure 1: Formation of water-soluble and biocompatible QD-micelles through an interfacially driven micro-emulsion process.

Key processes underlying the operation of individual neurons occur through the binding of neurotransmitter molecules with membrane receptors. Progress in understanding these phenomena requires biocompatible probes that detect neuronal processes within living animals (i.e. *in vivo*). We have successfully demonstrated that quantum dots (QDs) may be produced that allow fluorescence detection of neuronal voltage changes, and thus exhibit biocompatibility sufficient for their *in vivo* use for many behavioral neuroscience experiments. QDs are generally excellent for fluorescence labeling since they are very bright and stable in comparison with conventional organic dyes.

Monodisperse CdSe and CdSe/CdS core/shell QDs were synthesized through a "hot soap" injection process [1]. Phospholipids were used to encapsulate the QDs within a micelle core to form water-soluble and biocompatible QD micelles (Fig. 1) using an interfacially driven micro-emulsion process developed at Sandia [2,3]. The interdigitated surfactant layers surrounding the QDs resemble a bilayer structure that enable easy fusion of QDs into cell membranes. In this procedure, a concentrated suspension of QDs in chloroform is added to an aqueous solution containing a mixture of surfactants or phospholipids with different functional head groups such as ethylene glycol (-PEG) and amine ($-NH_2$). PEG is used to improve biocompatibility and amine groups provide sites for bioconjugation. Optical characterization of these biocompatible QD micelles indicated they maintained all the optical properies of the original hydrophobic QDs.

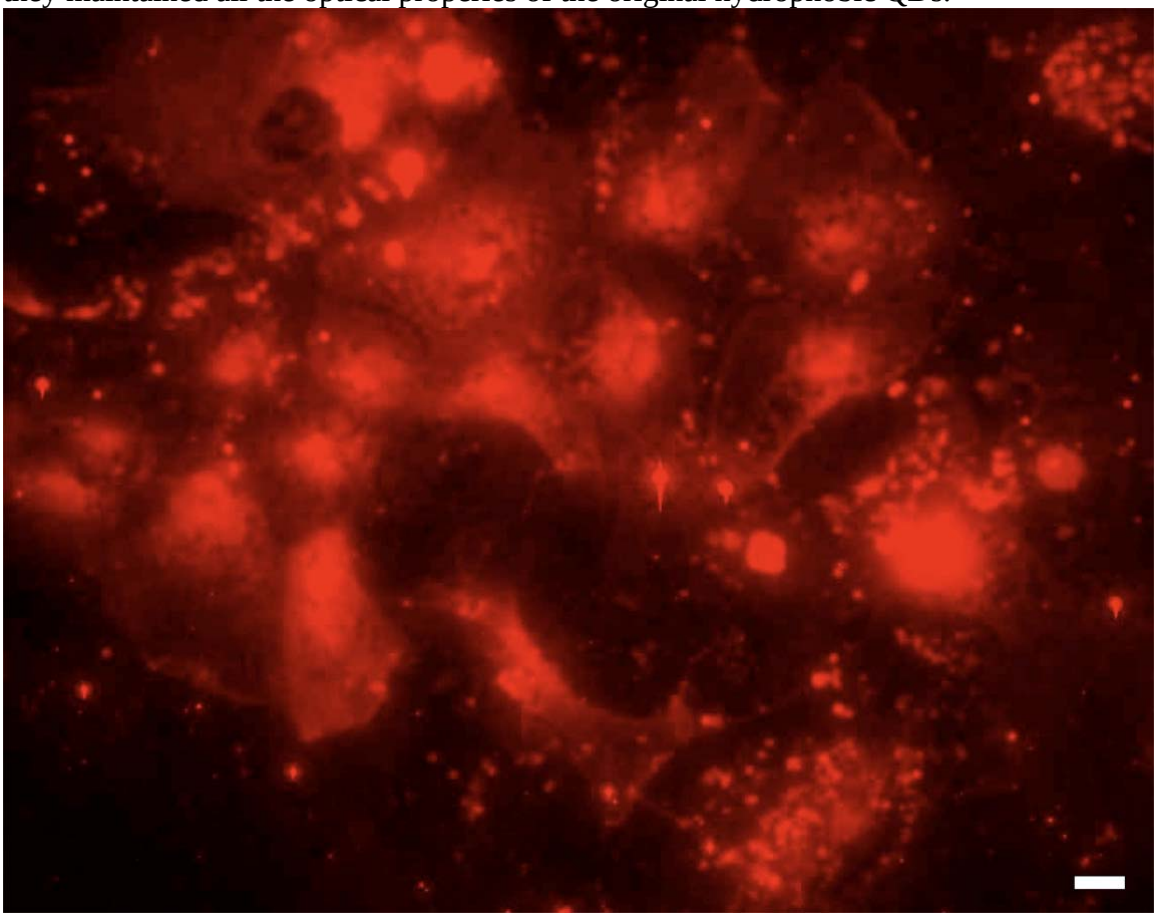

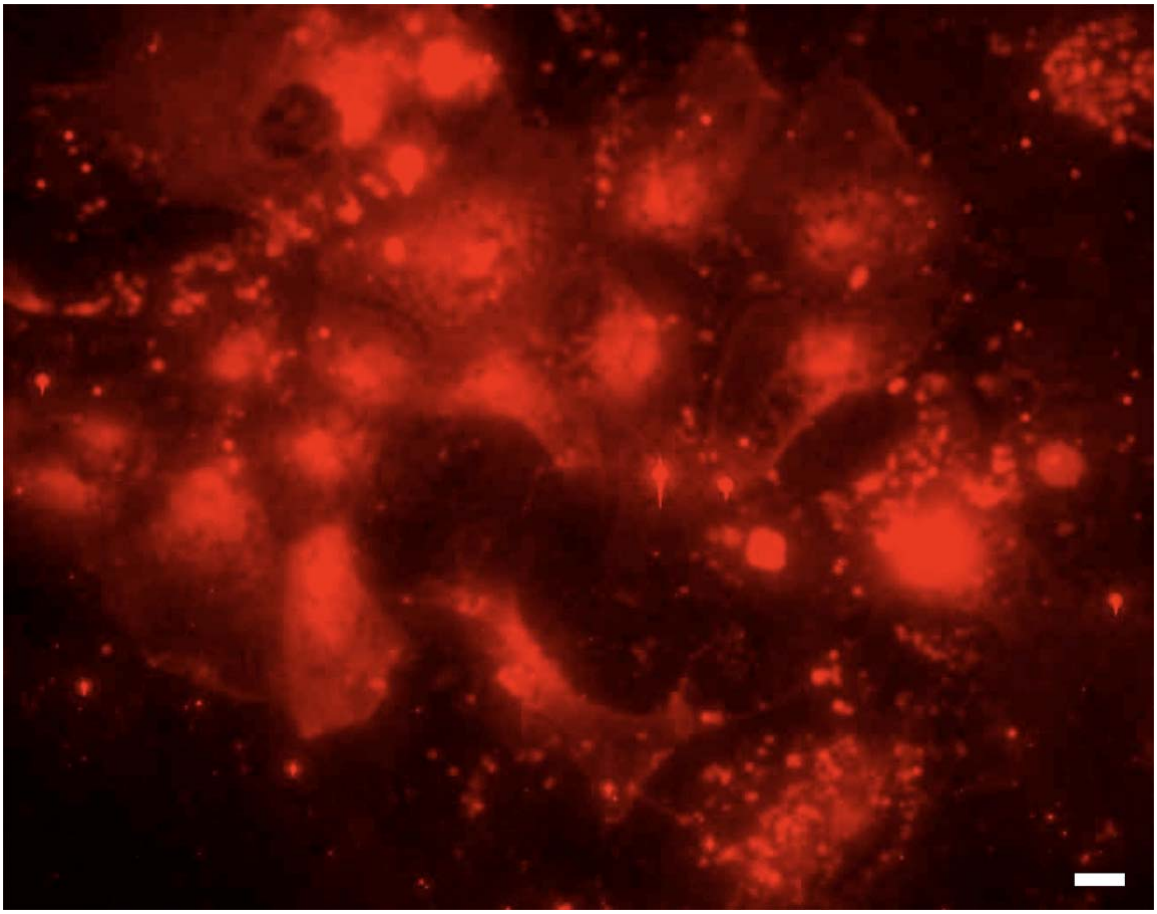

Figure 2: Fluorescence image of cultured hippocampal neurons from mouse brain exposed t QDs (590 nm emission). Scale bar =10 μm.

Sensing neuronal potential changes cross-membrane is based on the fluorescent intensity changes of those QDs that are close to or within neuronal membranes. Polarization of the local electric field across the neuronal membrane causes electron/hole pairs to be redistributed within each QD, resulting in an increase in fluorescence as detected by fluorescence imaging. Initial tests utilizing a QD micelle buffer solution to with cultured hippocampal pyramidal neurons demonstrated that the micelle bilayer structure promotes the adherence of nanoparticles to the lipid membrane of the neuron with QDs actually becoming wedged within the membrane (Figure 2). The biocompatibility of these QDs ensures the cells to be alive during measurements.survive a sufficient duration. The next step was to evaluate whether the quantum dots were sufficiently inserted into the membrane such that they would respond to a change in membrane voltage.

The resting membrane potential of hippocampal pyramidal neurons is largely determined by the equi-librium potential for K^+ and is typically –75 mV. From the Nernst Equation, adding 40 mM KCl to the solution bathing the neurons should change the membrane potential of the cell from –7575 mV to approximately –21 mV. LiveLive cell experiments using the QD treated cultured neurons showed a factor of 7 increase in fluorescence intensity in response to this membrane depolarization (Figure 3).

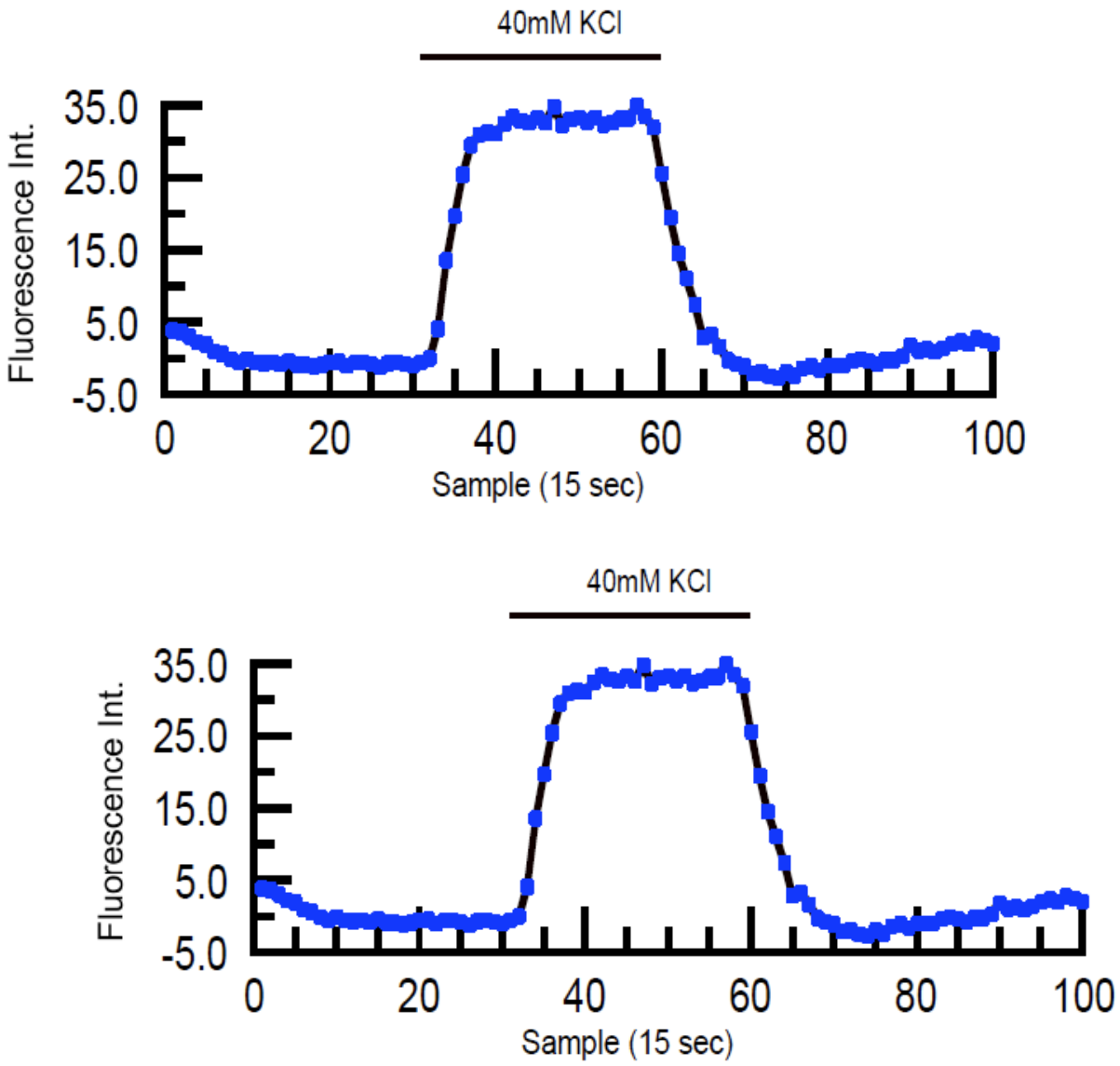

Figure 3: Fluorescence intensity trace of cultured neurons exposed to 590 nm QDs in a flow chamber of the imaging system. A region of interest was picked over a cell body, the average intensity was calculated, then baseline fluorescence was subtracted. The fluorescence intensity was recorded at 15 s time intervals. The fluorescence was allowed to stabilize in normal artificial cerebrospinal fluid (ACSF) for sample numbers 1-30, then 40 mM KCl was applied to the neurons between sample number 30-60, then washed with normal ACSF for sample numbers 60-100 (bar shows application of KCl)

This research demonstrates the use of QDs to detect neuronal voltage changes. QDs have distinct advantages over traditional voltage-indicating fluorescent dyes including high quantum yield and photostability. Further advances should provide the basis for larger scale measurement techniques (e.g., nanoelectrode arrays) essential to gaining an understanding of how nanoscale neural processes aggregate to produce phenomena at the micro (neuron-to-neuron interactions) and millimeter scales (neuronal network interactions).

We have discovered a new method in which spontaneous self-assembly is employed to synthesize monodisperse optically active nanoparticles with controlled size (< 50-nm), shape, tunable functionality, and enhanced solvent and thermal stability. Cooperative non-covalent interactions, such as hydrogen bonding and aromatic π-π stacking, assist self-assembly of amphiphilic macromolecules and structure directing agents (SDAs) to form both spherical and anisotropic solid polymer nanoparticles with SDAs residing in the particle core surrounded by the polymers. These nanoparticles are very stable, can be re-dispersed in common solvents forming homogenous solutions and ordered arrays upon solvent evaporation. These nanoparticles exhibit tunable optical properties upon choice of in accordance with SDAs. Our method is simple and general without requiringand does not require complicated synthetic chemistry, stabilizing surfactants, or annealing procedure (e.g., temperature or solvent annealing), making scalable synthesis practicable.

These monodisperse nanoparticles exhibit unique optical properties resulting form the used SDAs. Figure 4A and 4B show the UV-vis and fluorescent spectra of monodipserse nanoparticles respectively. The slight red-shifts in both B band (400-450450 nm) and Q band (600-700700 nm) again suggest the formation of j-aggregates through aromatic π-π stacking. The fluorescent spectra indicated remaining of indicates the optical emission for the nanoparticles. The optical property can be readily tuned without requiring complicated chemistry depending on the choice of SDAs. In addition to organic chromophores, the robustness of our self-assembly process enables us to prepare hybrid nanoparticles by using inorganic nanocrystals.

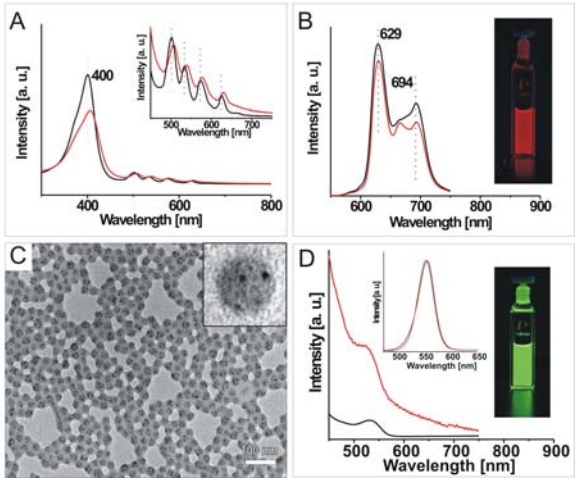

Figure 4: UV-vis absorption (A) and fluorescence (B) spectra of nanoparticles (red line) C, Representative TEM image of hybrid nanoparticles containing CdSe/ZnS semiconducting nanocrystals. D, UV-vis absorption and fluorescence (inset) spectra of CdSe/ZnS (black line) and polymer nanoparticles (red line). Optical pictures of emission from each

Figure 4C shows TEM image of the hybrid polymer nanoparticles that were prepared using $PS_{19.9k}$-$PVP_{29.4k}$ and hydroxyl group-functionalized CdSe/ZnS. The CdSe/ZnS nanocrystals were prepared according to Yang *et al*. The nanocrystals were then functionalized with hydroxyl (-OH) groups that are capable of forming hydrogen bonds with nitrogen (-N=) of PVP chains (Figure 1 process II). InsetThe inset TEM image highlights one polyer nanoparticles containing several CdSe/ZnS nanocrystals (~5-nm). Figure 4D compares UV-vis and fluorescent spectra of CdSe/ZnS nanocrystals and hybrid polymer nanoparticles. The optical absorption over 400-600600 nm and the emission between 600-600600 nm clearly demonstate that the hybrid polymer nanoparticle retain the optical property from CdSe/ZnS nanocrystals inside the nanoparticles.

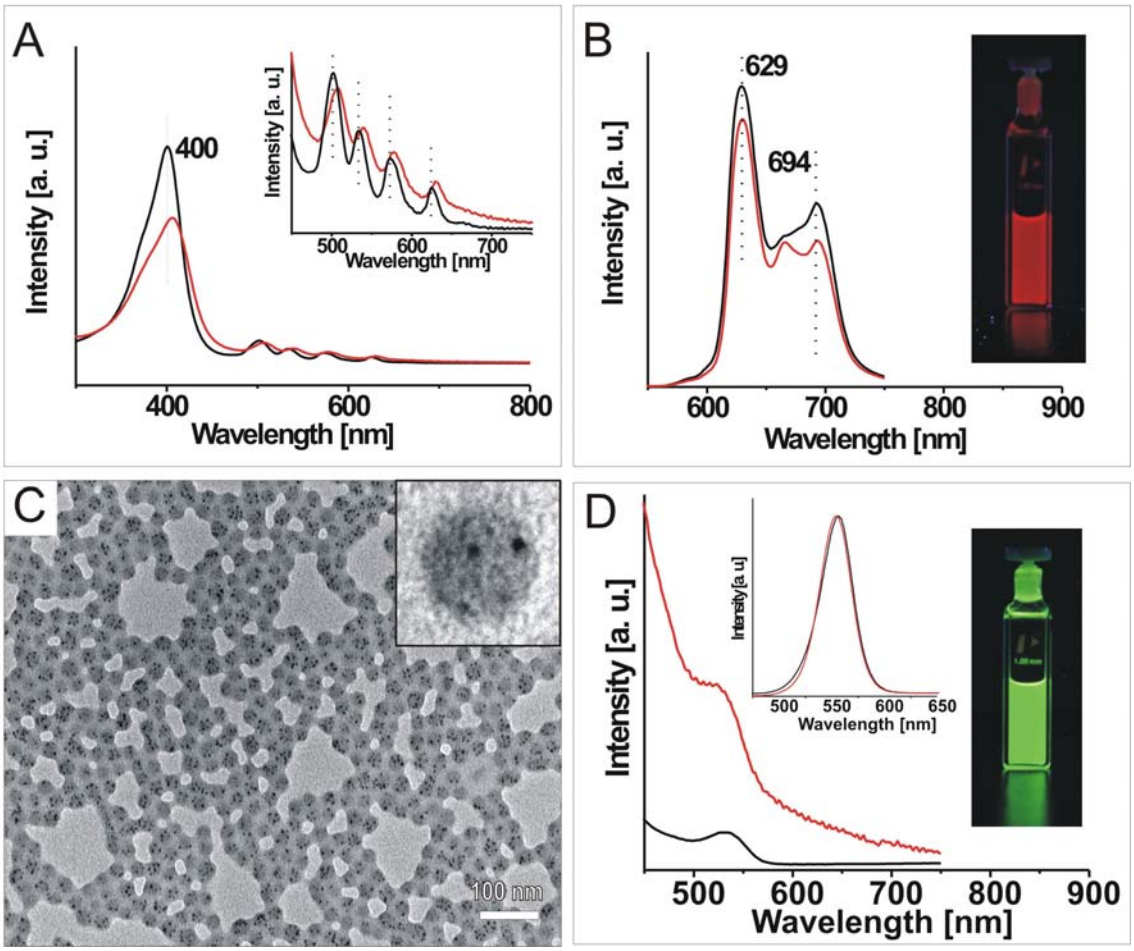

Figure 5: UV-vis absorption (A) and fluorescence (B) spectra of nanoparticles (red line) C, Representative TEM image of hybrid nanoparticles containing CdSe/ZnS semiconducting nanocrystals. D, UV-vis absorption and fluorescence (inset) spectra of CdSe/ZnS (black line) and polymer nanoparticles (red line). Optical pictures of emission from each composite nanoparticles solution are also shown.

4. SIMULATION FRAMEWORK

To simulate the transient behavior of neurons, model equations are used to describe the voltage potential as a function of the neuron's state. The membrane's voltage potential is a function of the type and distribution of the ion-channels active within the neuron. Two different membrane models were implemented which each of which describe a set of ion channels. First, the technically simpler, Hodgken-Huxley equations and next the more complex Connor-Stevens model. These membrane models were implemented to model both an area of neuron membrane and a length of a neuron cell, i.e. a length of neuron cable. In the following sections, we will describe the equations that were implemented and how they are solved in a typical simulation

Membrane Potential Equations

Given a section of neuron membrane, the voltage potential across the membrane (i.e. from inside to outside) is described by Koch [7] and Dayan [2]

$$C_m \frac{dV}{dt} = i_m + \frac{I_e}{A}$$

where C_m is the membrane capacitance, V is the voltage difference, t is time, i_m is the current through the membrane while I_e represents any externally applied current into the cell and A is the surface area of the membrane.

The membrane current is dependent on the type of ion channels within the membrane. In this work we implemented two standard models containing modeling sets of ion currents: the Hodgkin-Huxley model and the Connor-Stevens model.

Hodgkin-Huxley Model Equations

In the Hodgkin-Huxley model of membrane current, the current is described by:

$$i_m = i_{leak} + i_{Na} + i_K$$

where i_{leak} is the current that naturally leaks through the membrane, i_{Na} is the current associated with sodium ion channels and i_K is the current associated with potassium ion channels. This descriptive equation can be refined with algebraic expressions for the individual currents as:

$$i_m = \bar{g}_L (V - E_L) + \bar{g}_{Na} m^3 h (V - E_{Na}) + \bar{g}_K n^4 (V - E_K)$$

Parameters in this equation are: $\bar{g}_L$ is the maximal membrane conductance, E_L is the membrane reversing potential, $\bar{g}_{Na}$ is the sodium ion channel conductance, E_{Na} is the sodium channel reversing potential while $\bar{g}_K$ and E_K are the potassium channel maximal conductance and reversing potential respectively. The variables, m, h and n are voltage dependent gating

variables that model the relative availability of the sodium and potassium channels. Gating variables, m, h and n are described by the ordinary differential equations:

$$\frac{dm}{dt} = \alpha_m(V)\cdot(1-m) - \beta_m(V)\cdot m$$
$$\frac{dh}{dt} = \alpha_h(V)\cdot(1-h) - \beta_h(V)\cdot h$$
$$\frac{dn}{dt} = \alpha_n(V)\cdot(1-n) - \beta_n(V)\cdot n$$

The voltage dependent coefficients, $\alpha(V)$ and $\beta(V)$ are:

$$\alpha_m(V) = \frac{0.1(V+40)}{1-e^{-0.1(V+40)}}$$
$$\beta_m(V) = 4e^{-0.0556(V+65)}$$
$$\alpha_h(V) = 0.07e^{-0.05(V+65)}$$
$$\beta_h(V) = \frac{1}{1+e^{-0.1(V+35)}}$$
$$\alpha_n(V) = \frac{0.1(V+55)}{1-e^{-0.1(V+55)}}$$
$$\beta_n(V) = 0.125e^{-0.0125(V+65)}$$

Note, in the equations for m, h and n, the voltage is given in units of milli-volts and time in milli-seconds.

Connor-Stevens Model Equations

To more accurately simulate the diverse set of currents that work in typical neurons, the Connor-Stevens model adds two additional current terms to the membrane current equation:

$$i_m = \bar{g}_L(V-E_L) + \bar{g}_{Na}m^3h(V-E_{Na}) + \bar{g}_K n^4(V-E_K) + \bar{g}_A a^3 b(V-E_A) + \bar{g}_{CaT}M^2H(V-E_{Ca}) + \bar{g}_{KCa}c^4(V-E_K)$$

where the maximal conductance and reversal potentials, $\bar{g}_A$, E_A, $\bar{g}_{CaT}$, E_{Ca}, $\bar{g}_{KCa}$ and E_K are for the A-current, transient calcium current and calcium dependent potassium current respectively.

Gating variables for the additional current terms are described by:

Gating variable a

$$\frac{da}{dt} = \frac{a_\infty(V) - a}{\tau_a(V)}$$

and

$$a_\infty(V) = \left(\frac{0.0761 e^{0.0314(V+94.22)}}{1+e^{0.0346(V+1.17)}} \right)^{\frac{1}{3}}$$

$$\tau_a(V) = 0.3632 + \frac{1.158}{1+e^{0.0497(V+55.96)}}$$

Gating variable b

$$\frac{db}{dt} = \frac{b_\infty(V) - b}{\tau_b(V)}$$

and

$$b_\infty(V) = \left(\frac{1}{1+e^{0.0688(V+53.3)}} \right)^4$$

$$\tau_b(V) = 1.24 + \frac{2.678}{1+e^{0.0624(V+50)}}$$

Gating variable M

$$\frac{dM}{dt} = \frac{M_\infty(V) - M}{\tau_M(V)}$$

and

$$M_\infty(V) = \frac{1}{1+e^{\frac{-(V+57)}{6.2}}}$$

$$\tau_M(V) = 0.612 + \frac{1}{e^{\frac{-(V+132)}{16.7}} + e^{\frac{(V+16.8)}{18.2}}}$$

Gating variable H

$$\frac{dH}{dt} = \frac{H_\infty(V) - H}{\tau_H(V)}$$

and

$$H_\infty(V) = \frac{1}{1 + e^{\frac{(V+81)}{4}}}$$

$$\tau_H(V) = \begin{cases} e^{\frac{V+467}{66.6}} & V < -80mV \\ 28 + e^{\frac{-(V+22)}{10.5}} & V \geq -80mV \end{cases}$$

Gating variable c

$$\frac{dc}{dt} = \frac{c_\infty(V) - c}{\tau_c(V)}$$

and

$$c_\infty(V) = \left(\frac{\left[Ca^{2+}\right]}{\left[Ca^{2+}\right] + 3\mu M} \right) \frac{1}{1 + e^{\frac{-(V+28.3)}{12.6}}}$$

$$\tau_c(V) = 90.3 - \frac{75.1}{1 + e^{\frac{-(V+46)}{22.7}}}$$

As in the case of the Hodgken-Huxley model's gating variables, the gating variable equations stated above use voltage in milli-volts and time in milli-seconds and calcium ion concentration in micro-moles for unit consistency.

Cable Model Equations

To model a section of a neuron process, such as an axon, a *cable-equation* formulation is used. Here, the cable equation is specified as:

The following equation was used to model the cable properties of the neuron:

$$C_m \frac{dV_i}{dt} = -i_i^m + \frac{I_i^E}{A_i} + g_{i,i+1}(V_{i+1} - V_i) + g_{i,i-1}(V_{i-1} - V_i)$$

where C_m is the membrane capacitance, V_i is the voltage in compartment i relative to an external ground, t is time, i_i^m is the current through the membrane in compartment i, I_i^E represents any externally applied current into the cell and A_i is the surface area of the membrane in compartment i. The final two terms represent current flow into the adjoining compartments, $i-1$, for the previous compartment and $i+1$ for the next compartment. Conductance between the compartments, $g_{i,i+1}$ and $g_{i,i-1}$ can be calculated by:

$$g_{i,j} = \frac{a_i a_j^2}{r_{Long} L_i \left(L_i a_j^2 + L_j a_i^2 \right)}$$

where a_i is the radius of compartment i, L_i is the length of compartment i and r_{Long} is the longitudinal intracellular resistance.

Model Equation Implementation

The model equations in the previous sections were implemented in the Xyce Electrical Circuit Simulator [6]. Verification of the model equation behavior consisted of simulating a patch of neuron membrane under an applied current input. Gating variables and trans-membrane currents were then compared to exiting calculations in Koch [7]. An example of the typical output using physical parameters from the giant squid axon is a follows:

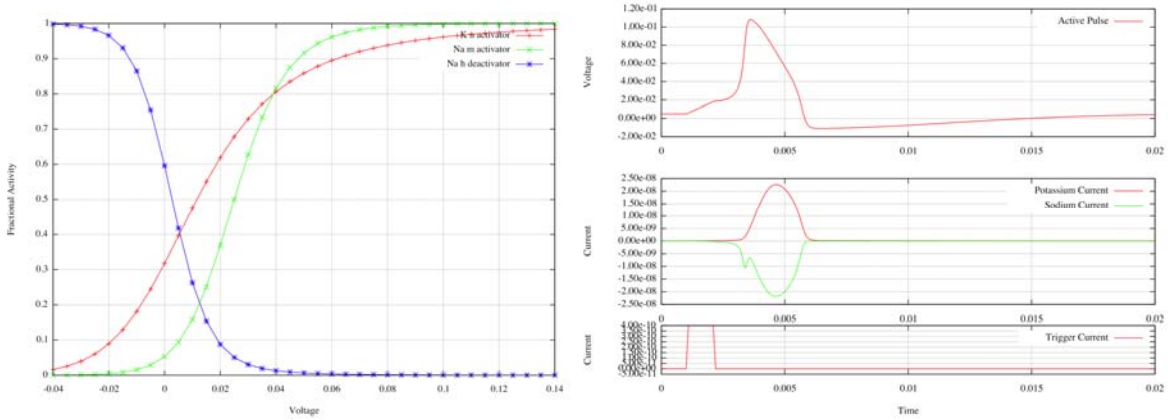

Figure 6: Gating variables and Sodium and Potassium channel currents

Additionally, a test of Xyce's ability to handle a naturally derived topology was devised. For this test we simulated the topological connectivity of C. elegans. While the connectivity data for the neurons is known, the spatial positioning was not. Therefore this was a verification exercise in the simulation of a complexly interconnected network.

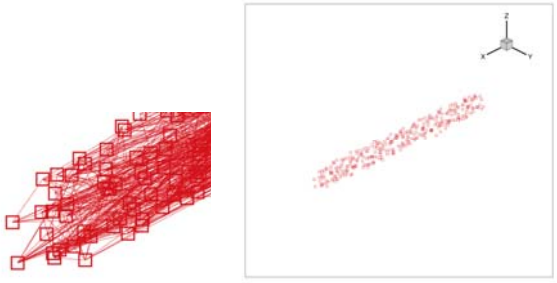

Figure 7: Individual neuron centers and zoomed in connectivity view

Figure 7 shows the individual centers of the neurons used in this simulation and the zoomed in view is an example of the degree of the connectivity of the neurons. For this simulation, Hodgkin-Huxley membrane equations were used.

C. elegans Neural Simulation

Our initial goal was to model the effects of serotonin on C. elegans egg-laying.

Conceptual model of egg-laying

The HSN neurons synapse on the vulval muscles, and control their activity by release of the neurotransmitter serotonin. In *C. elegans* lacking HSNs or incapable of producing serotonin, exogeneous serotonin can stimulate egg-laying [4].

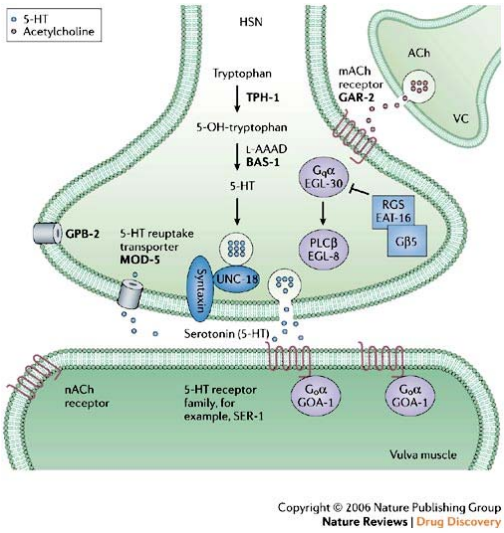

Figure 8: From Kaletta and Hengartner [4]

There are a number of other neurons also involved in egg-laying, but HSN is thought to be key. A schematic of the egg-laying circuit is shown

below.

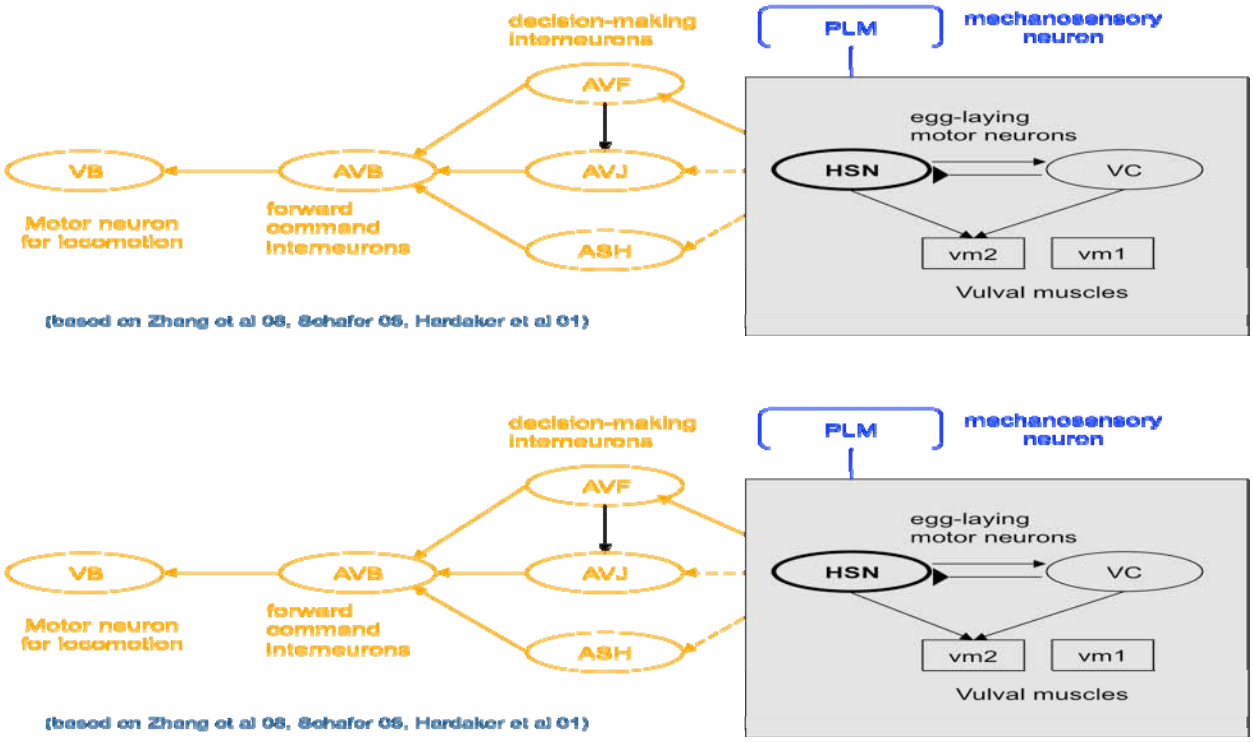

Figure 9: HSN system From Zhang et al [10]
The core of the egg-laying motor circuit in C. elegans, shown in the boxed area, is a common microcircuit motif including feedforward excitation and feedback inhibition. Understanding its functional properties may aid understanding of more complex systems that include this microcircuit.

Zhang et al [10] showed that HSN neurons exhibit intrinsic Ca oscillations which appear to be correlated with egg-laying. There are some phenomenological models of egg-laying activity that suggest various regulatory interactions between HSN and VC (e.g. Waggoner et al [9]).
Our intent was to start by capturing the intrinsic activity in HSNs, and then add modulation by serotonin and/or other neurons in the circuit. We did not intend to model the vulval muscles or egg-laying itself, on the assumption that action potentials in the HSN are correlated with these events and measuring those action potentials would be sufficient for comparison to the experiments.

Neural activity in HSNs

There have been no electrophysiological recordings of HSNs. *C. elegans* neurons are generally very small and difficult to access; the primary paper on electrophysiology in *C. elegans* [4]

focused on one particular neuron, but showed some evidence that other neurons had similar properties.

C. elegans does not contain the gene to produce the sodium channel responsible for action potentials in most other animals [1,3]. Since neurons in this animal are very small and nearly isopotential, they may be able to transmit signals passively, without the regeneration that sodium-based action potentials provide [4]. However, there is evidence of Ca-based action potentials in some *C. elegans* neurons [8].

C. elegans does have a wide variety of potassium channels, and a smaller variety of calcium channel types [1]. We felt that we could model HSN activity with the K and Ca channels present in the Xyce implementation of the Connor-Stevens model, tuned to produce the activity reported in the literature and/or recorded during the experiments associated with this project.
On closer examination, this approached turned out was judged to be somewhat naïve. There are some general ideas of what kinds of channels these neurons use, but insufficient data to resolve discrepancies. Goodman et al [3] determined that their data supported activity from at least a calcium channel, a transient potassium channel, and a persistent potassium channel. They did not characterize exactly which types of each of these channels they thought were present, but their data do show approximate ranges of membrane voltages for which these channels are active, and some quantitative characteristics of their activation and inactivation. Shtonda and Avery [8] claim that action potentials in *C. elegans* involve an L-type calcium channel, a T-type calcium channel, and a potassium channel.

There is a published computational model of basic *C. elegans* neuron ion channels that we intended to build on. Sakata and Shingai [5] chose to use just one calcium channel and one potassium channel, as the minimum necessary to account for experimental results. Their potassium channel is somewhat similar to the A-current included in the Connor-Stevens model. However, their calcium channel is a Ca-dependent Ca channel that is not one of the standard currents included in the devices implemented in Xyce. There is also some confusion about the the parameters used in the Sakata and Shingai paper, not all parameters are given, and some values conflict with values in their references.

Using the calcium and potassium channels available in the Xyce devices, we did attempt to reproduce some of the certain results seen in Goodman's experiments [3]. However, this is when these simulations revealed that both types of channels are active over a very different range of membrane voltages than the model channels implemented in the Xyce devices. Also, it is proposed that the positive feedback provided by the calcium-dependence of the calcium channel in Sakata and Shingai is probably important for getting an amplified response to injected current, but this mechanism is not available in our (current) simulated devices.

4. EXPERIMENTAL SYSTEM

To determine if PEG-coated nanoparticles could be used to monitor neural activity in vivo, the nanoparticles were injected into *C. elegans* hermaphrodites in the vicinity of the HSN. Nomarski microscopy was used to identify the position of the HSN within *C. elegans* and standard microinjection procedures were employed [11]. The nanoparticle solution (undiluted) was centrifuged for 1 min at 12,000RPM to remove any clumps that would otherwise clog the injection needles. *mgIs42* transgenic animals were injected as they express a GFP reporter in the HSN cell body and axon ([12]; Figure 10), enabling us to use fluorescence microscopy to determine localization of the nanoparticles with respect to the HSN.

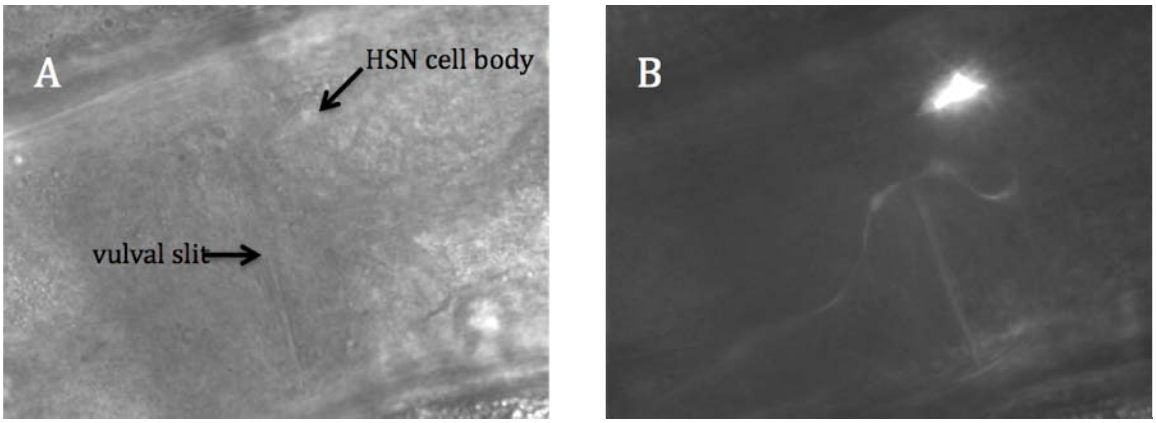

Figure 10: mgIs42 animals can be used to visialize the HSN neuron and cell body by GFP expression. (A) Bright field Nomarski image of the midbody of a *C. elegans* hermaphrodite. (B) GFP expression within the HSN cell body and axon.

Following microinjection, fluorescence Nomarski microscopy was used to determine the cellular targeting of the PEG-coated nanoparticles with respect to the HSN. Figure 11 pictures an example of an injected animal. In general, the nanoparticles could be found localized to the vicinity of the HSN, but were not observed to localize within the HSN membrane (n=25).

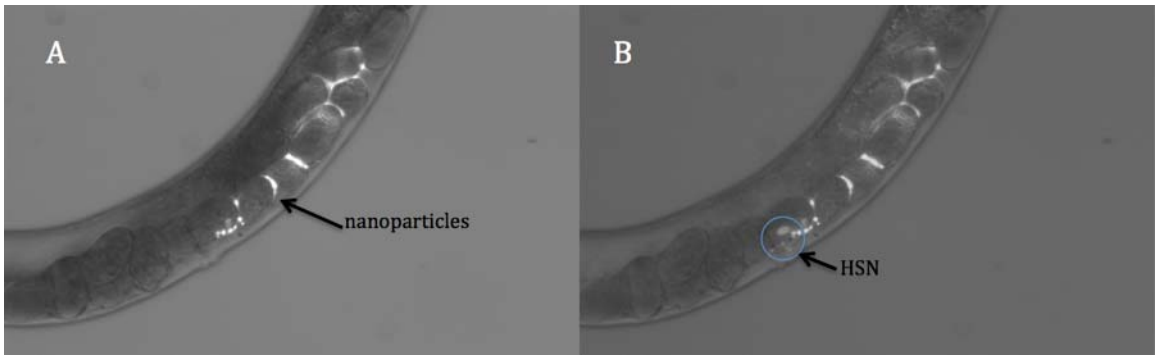

Figure 11: Nanoparticles localize to the vicinity of the HSN in microinjected mgIs42 animals. (A) Fluorescent nanoparticles dispersed within the midbody of the hermaphrodite. Nanoparticle fluorescence is observed using an RFP filter. (B) An overlay with an image of the same animal observed with a GFP filter shows the relative position of the HSN cell body and axon (circled).

The HSN neurons synapse on the vulval muscles, and control their activity by release of the neurotransmitter serotonin. Application of exogenous serotonin can induce egg-laying activity via stimulation of HSN neural activity (reviewed in [13]). Our goal was to determine if we could detect neural activity (depolarization) of the HSNs, in resting animals, or following addition of exogenous serotonin, by a shift in fluorescent emission of the nanoparticles. While we did not reach our goal, our results are promising; with better targeting of the nanoparticles, it is possible our goal could be achieved. Use of PEG-coated nanoparticles greatly improved biocompatibility and dispersion of the nanoparticles in vivo; in earlier injection studies, we found that nanoparticles without a PEG coating aggregated within the extracellular matrices of the animals (data not shown). Many groups have attempted to use functionalized nanoparticles containing QDs for *in vivo* applications with limited success. Achievement of our goal would represent a significant advance in the field of *in vivo* neural imaging.

5. CONCLUSIONS

Through this project Sandia has advanced the state-of-the-art with respect to technical capabilities essential to nanoscale scientific studies of neuronal processes. Capabilities have been developed to engineer biocompatible nanoparticles that respond with differential florescence within the voltage range typically observed with neuron action potentials. These same nanoparticles may be biofunctionalized to enable their response to a variety of neuronal phenomenon.

Of particular significance, the use of nanoparticles for recording nanoscale neuronal responses has been demonstrated within an *in vivo* animal experimental protocol. To the author's knowledge, this is the first occasion on which this achievement has been demonstrated, with past research using neuronal tissue being restricted to cell cultures, and other less naturalistic paradigms.

Finally, capabilities have been developed to model nanoscale neuronal phenomenon within a massively parallel computing simulation. While not exercised using data obtained through the current project, this capability provides the foundation for future work modeling multi-scale neuronal processes.

4. REFERENCES

1. Cornelia I. Bargmann, "Neurobiology of the Caenorhabditis elegans Genome," *Science* 282, no. 5396 (December 11, 1998): 2028-2033, doi:10.1126/science.282.5396.2028.
2. Dayan, Peter & Abbott L. F., "Theoretical Neuroscience: Computational and Mathematical Modeling of Neural Systems" MIT Press, Cambridge Massachusetts 2001.
3. Miriam B Goodman et al., "Active Currents Regulate Sensitivity and Dynamic Range in C. elegans Neurons," *Neuron* 20, no. 4 (April 1998): 763-772, doi:10.1016/S0896-6273(00)81014-4.
4. Titus Kaletta and Michael O. Hengartner, "Finding function in novel targets: C. elegans as a model organism," *Nat Rev Drug Discov* 5, no. 5 (May 2006): 387-399, doi:10.1038/nrd2031.
5. Kazumi Sakata and Ryuzo Shingai, "Neural network model to generate head swing in locomotion of Caenorhabditis elegans," *Network: Computation in Neural Systems* 15, no. 3 (2004): 199-216.
6. Eric R. Keiter, Ting Mei, Thomas V. Russo, Eric L. Rankin, Roger P. Pawlowski, Richard L. Schiek, Keith R. Santarelli, Todd S. Coffey, Heidi K. Thornquist, Deborah A. Fixel, "Xyce Parallel Electronic Circuit Simulator", SAND2009-5871 Sandia National Laboratories, Albuquerque, NM (SRD), September 2009.
7. Koch, Christof, "Biophysics of Computation: Information Processing in Single Neurons," Oxford University Press, 1998.
8. Boris Shtonda and Leon Avery, "CCA-1, EGL-19 and EXP-2 currents shape action potentials in the Caenorhabditis elegans pharynx," *J Exp Biol* 208, no. 11 (June 1, 2005): 2177-2190, doi:10.1242/jeb.01615.
9. Laura E. Waggoner et al., "Control of Alternative Behavioral States by Serotonin in Caenorhabditis elegans," *Neuron* 21, no. 1 (July 1998): 203-214, doi:10.1016/S0896-6273(00)80527-9.
10. Mi Zhang et al., "A Self-Regulating Feed-Forward Circuit Controlling C. elegans Egg-Laying Behavior," *Current Biology* 18, no. 19 (October 14, 2008): 1445-1455, doi:10.1016/j.cub.2008.08.047.
11. Evans, T. C., ed. Transformation and microinjection (April 6, 2006), *WormBook*, ed. The *C. elegans* Research Community, WormBook, doi/10.1895/ wormbook.1.108.1, http://www.wormbook.org.
12. Sze, J.Y., et al., "Food and metabolic signaling defects in a Caenorhabditis elegans serotonin-synthesis mutant," Nature 403, no. 6769 (February 3, 2000): 560-4.
13. Schafer, W. R. Egg-laying (December 14, 2005), *WormBook*, ed. The *C. elegans* Research Community, WormBook, doi/10.1895/wormbook.1.38.1, http://www.wormbook.org.

DISTRIBUTION

Unless otherwise noted, all copies are distributed electronically.

1	MS0123	D. Chavez, LDRD Office	1011
1	MS0316	Richard Schiek	1437
1	MS0892	Conrad James	1714
1	MS1188	Chris Forsythe	6341
1	MS1188	Christy Warrender	6343
1	MS1349	Hongyou Fan	1815
1	MS9291	Cathy Branda	8621
1	MS0899	Technical Library	9536


Sandia National Laboratories